ACS Sustainable Chemistry & Engineering

pubs.acs.org/journal/ascecg

Research Article

Catalytic Fast Pyrolysis of Biomass: Catalyst Characterization Reveals the Feed-Dependent Deactivation of a Technical ZSM-5-Based Catalyst

Beatriz Luna-Murillo,[#] Mehmet Pala,*[,#] Alessandra Lucini Paioni, Marc Baldus, Frederik Ronsse, Wolter Prins, Pieter C. A. Bruijnincx, and Bert M. Weckhuysen*

Cite This: https://dx.doi.org/10.1021/acssuschemeng.0c07153

Read Online

ACCESS | Metrics & More | Article Recommendations | Supporting Information

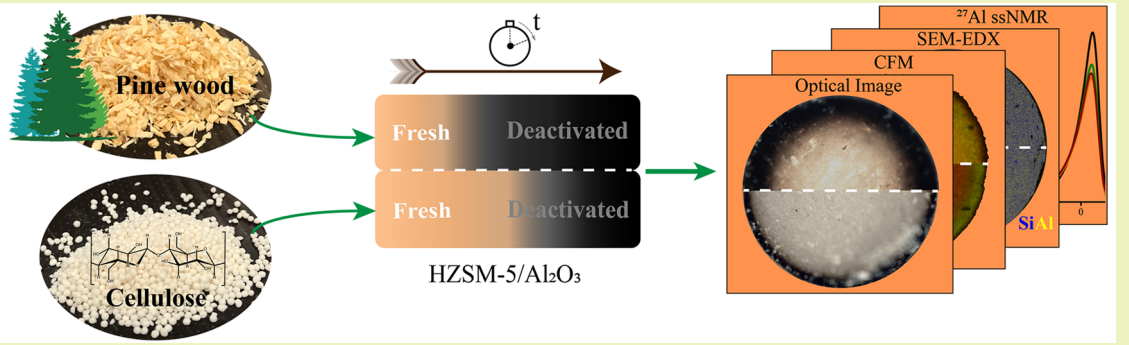

ABSTRACT: Catalyst deactivation due to coking is a major challenge in the catalytic fast pyrolysis (CFP) of biomass. Here, a multitechnique investigation of a technical Al_2O_3-bound ZSM-5-based extrudate catalyst, used for the CFP of pine wood and cellulose (at a reactor temperature of 500 °C), provided insight into the effects of extrusion, the catalytic pyrolysis process, and catalyst regeneration on the catalyst structure. As a result of a reduction in acidity and surface area due to the coking catalyst, the activity dropped drastically with increasing time-on-stream (TOS), as evidenced by a decrease in aromatics yield. Strikingly, confocal fluorescence microscopy at the single-particle level revealed that vapor components derived from whole biomass or just the cellulose component coke differently. While pine-wood-derived species mainly blocked the external area of the catalyst particle, larger carbon deposits were formed inside the catalyst's micropores with cellulose-derived species. Pyridine FT-IR and solid-state NMR spectroscopy demonstrated irreversible changes after regeneration, likely due to partial dealumination. Taken together with <30 g kg^{-1} aromatics yield on a feed basis, the results show a mismatch between biomass pyrolysis vapors and the technical catalyst used due to a complex interplay of mass transfer limitations and CFP chemistry.

KEYWORDS: *Catalytic pyrolysis, Biomass, Zeolite ZSM-5, Alumina, BTX, Spectroscopy, Catalyst deactivation*

INTRODUCTION

Catalytic fast pyrolysis (CFP) is a thermochemical upgrading technology that enables the production of BTX (Benzene, Toluene, and Xylenes) aromatics, polycyclic aromatic hydrocarbons (e.g., naphthalene and derivatives) and C_2-C_3 olefins from lignocellulosic biomass.[1,2] A considerable amount of research on the CFP of biomass has been performed over the past few decades,[3−6] aiming the use of the produced hydrocarbons either toward gasoline-range blending components or toward a source of base chemicals. Zeolite ZSM-5 generally shows a superior performance in catalytic upgrading of oxygenate-containing vapors[7,8] and is typically the catalyst material of choice for BTX production from biomass. Despite the promising advances shown by ZSM-5 catalyzed CFP, the process is also characterized by low carbon yields and rapid catalyst deactivation as a result of excessive coke formation.[9,10] More insight is needed into the nature and spatiotemporal development of the pyrolysis vapor-derived coke formed on the catalyst to ultimately reduce the loss of carbon through the design of a more robust catalyst.

The conversion of biomass-derived oxygenates to hydrocarbons has drawn inspiration from zeolite-based catalysis in, e.g., the methanol-to-hydrocarbons (MTH) type processes.[11,12] Consequently, this led to the idea that, similar to MTH, the mechanism of biomass CFP also proceeds through a

Received: September 29, 2020
Revised: November 21, 2020

hydrocarbon-pool mechanism.[13] According to this view, oxygenated pyrolysis vapors follow a series of cracking and dehydration reactions to produce small olefins inside the zeolite micropores followed by aromatization.[14−16] Analogously, coke formation mechanisms in biomass CFP would then be expected to also be similar to MTH. In the MTH process, highly methylated monoaromatics are produced through the dual-cycle mechanism over zeolite-based catalysts,[17] which then lead to the formation of condensed coke precursors.[18] However, catalyst deactivation with biomass pyrolysis vapors[10] is more rapid than in MTH,[19] implying that this analogy may not hold. Indeed, to improve biomass CFP efficiency, thorough analysis of the nature and the location of coke deposits formed upon CFP of biomass and their impact on (ir)reversible changes in catalyst structure is required, in particular for shaped catalyst extrudates.

An in-depth characterization of the catalyst, pre/post-reaction and after regeneration, could shed light on that issue. From a feedstock perspective, fragments of the original polymeric components of lignocellulose present in the pyrolysis vapors (i.e., those derived primarily from the lignin fraction) are too large[20] to be able to diffuse into the micropores of the zeolite. Wang et al.[21] indeed reported that aromatic hydrocarbon yield in micropyrolysis tests decreased in the order of cellulose (29.8 C%) > hemicellulose (19.4 C%) ≫ lignin (7.4 C%). They also found that the yield of catalytic coke was the highest with cellulose (30% on carbon basis), while with lignin, thermal production of coke by condensation seemed to contribute more to the solid carbonaceous residue. Stanton et al.[22] recently showed that lignin-derived vapors contributed less to catalyst deactivation by irreversible structural changes in a technical zeolite ZSM-5-based catalyst than that of cellulose-derived vapors did, as evidenced by the higher amounts of acid sites (76%) and micropore area (93%) retained on the catalyst following regeneration after the CFP of lignin. Together, these studies suggest that lignin-derived monomers and oligomers coke on the external surface, while cellulose-derived vapors coke via successive aromatization inside the micropores.

Previous studies[21,23] have shown that the (powdered) bulk zeolite material is far too active for efficient oxygenates-to-hydrocarbon conversion, giving extensive coke formation instead. Shaped catalysts, in which the active zeolite phase is diluted in other (binder) components, are, however, typically applied industrial practice to achieve optimal physical and chemical performance in real-life industrial reactors, whether it is a fluidized bed or an *ex situ* fixed-bed reactor. Technical catalysts, for example, provide mechanical strength, and avoid excessive pressure drops inside the reactor vessels.[24,25] As binder addition also leads to alteration of the material's physicochemical properties (e.g., mass transport, acidity), it is of paramount importance to also study the performance of such shaped catalyst materials in biomass CFP. For example, typical binder materials such as alumina (Al_2O_3), silica (SiO_2), or clays can alter catalytic activity by additional precracking of larger oligomers taking place in the binder matrix. Mesoporous Al_2O_3 binders have been shown to improve robustness and add precracking activity in diverse catalytic processes when compared to technical catalysts made with inert SiO_2 binders.[26−28] Studies at the single particle catalyst level previously already showed that (micro)spectroscopic spatio-temporal studies can provide critical information on the accessibility, predominant active sites, and possible deactivation pathways of zeolite ZSM-5-based catalyst materials in different complex matrices including fluid catalytic cracking and CFP catalysts.[28−30] For example, Heracleous et al.[31] recently reported on the nature and location of carbon deposits formed within technical ZSM-5-based catalyst extrudates upon CFP of biomass, using novel catalyst formulation of ZrO_2 incorporated nanocrystalline ZSM-5, agglomerated with attapulgite. As such, it may not be straightforward to decouple the influence of individual components (ZrO_2, nanocrystalline zeolite, and the attapulgite clay) on coke formation.

Literature dealing with a detailed characterization of the catalyst properties along with bench scale CFP testing is in general scarce, however. Using a multitechnique characterization approach covering multiple length scales,[32] we here study the structure−performance relations governing ZSM-5/Al_2O_3 technical catalysts for the CFP of pine and cellulose biomass. Bench-scale experiments were performed in a continuously fed fast pyrolysis system that enabled *ex-situ* upgrading of pyrolysis vapors over a fixed-bed of the catalyst. Yields and bio-oil compositions were determined for the fresh and the regenerated catalyst to investigate the effect of reaction and regeneration. Catalyst performance could thus be correlated with the (spatially resolved) physicochemical properties. The extensive analysis of the catalysts revealed the mismatch between the biomass pyrolysis vapors and the catalyst system due to a complex interplay of mass transfer limitations and CFP chemistry. Also, different catalytic mechanisms seem to dominate pine and cellulose CFP.

EXPERIMENTAL SECTION

Biomass. Pine wood (Bemap Houtmeel B.V., Bemmel, The Netherlands) with a particle size range of 1.0−2.0 mm and cellulose (Cellets 1000, Pharmatrans Sanaq AG, spherical pellets) with a particle size range of 1.0−1.4 mm were used as feedstock materials in the catalytic and noncatalytic fast pyrolysis experiments. The pine wood feedstock had an elemental composition of 0.47 g g^{-1} C, 0.06 g g^{-1} H, and 0.46 g g^{-1} O on a dry basis. The biochemical composition of the pine wood used is 0.35 g g^{-1} cellulose, 0.29 g g^{-1} hemicellulose, and 0.28 g g^{-1} lignin (on dry biomass basis). The cellulose feedstock contained 0.42 g g^{-1}C, 0.06 g g^{-1} H, and 0.52 g g^{-1}O. The feedstocks used within this study, pine wood and cellulose, are denoted as PW and CELL, respectively.

Catalyst Synthesis. HZSM-5/Al_2O_3 composites were prepared by mixing alumina powder (PURAL SB from Sasol), ZSM-5 powder (CBV 2314 from Zeolyst, with SiO_2/Al_2O_3 = 23), water, and an aqueous acid solution in a kneader for about 60 min at room temperature. Subsequently, the obtained paste is passed through an extruder to obtain the extrudates in a spaghetti-like structure. Afterward, extrudates were dried at room temperature overnight. The dry catalyst extrudates were then crushed to obtain a particle size between 1.0 and 3.0 mm, which was followed by a calcination sequence, first at 350 °C for 16 h and then at 600 °C for 16 h. The composites obtained contained 50% zeolite ZSM-5 and 50% alumina by weight. While fresh catalyst extrudates are denoted as HZSM-5/Al_2O_3 throughout the manuscript, the individual zeolite and binder powders are denoted as HZSM-5 and Al_2O_3, respectively. Prior to any characterization, the individual components of the extrudates, HZSM-5 and Al_2O_3, were also subjected to the same two-step calcination procedure mentioned above.

Catalyst Characterization. A large variety of analytical techniques has been used to extensively characterize the fresh, spent, and regenerated technical ZSM-5-based catalyst extrudates used in this work. Physicochemical properties of the HZSM-5/Al_2O_3 extrudate catalyst were investigated by X-ray diffraction (XRD), Ar physisorption, Hg porosimetry, (FIB)-SEM-EDX, NH_3-TPD, FT-IR spectroscopy, and ^{27}Al solid state NMR (ss-NMR). Analysis of the

https://dx.doi.org/10.1021/acssuschemeng.0c07153
ACS Sustainable Chem. Eng. XXXX, XXX, XXX−XXX

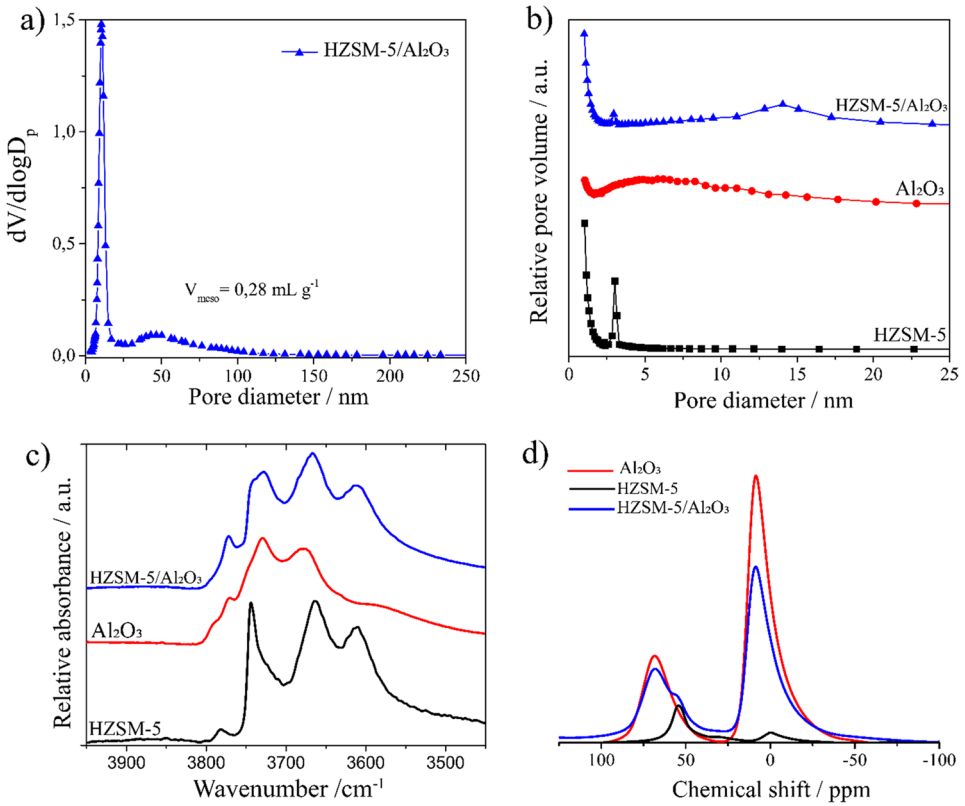

Figure 1. Pore size distribution graphs after (a) Hg porosimetry and (b) Ar physisorption at −196 °C. (c) Fourier transform-infrared (FT-IR) spectra of the OH-stretching region. (d) ^{27}Al solid state nuclear magnetic resonance (ss-NMR) of fresh, individual components and the HZSM-5/Al_2O_3 catalyst extrudates. The intensities in the ss-NMR spectra were normalized by weight.

coke deposits (i.e., nature and location of carbon deposits) has been carried out by Temperature-Programmed Oxidation (TPO) with online Mass Spectrometry (MS) and Confocal Fluorescence microscopy (CFM). Experimental details are given in the Supporting Information.

Spent catalyst extrudates were collected at 10, 60, and 180 min time-on-stream after catalytic pyrolysis tests, and they were analyzed without further treatment, unless otherwise stated. It should be noted here that no apparent coke gradient was observed along the axial direction of the catalyst bed at the end of our experiments. Therefore, it is assumed that the use of a fixed-bed configuration for the catalytic reactor does not conceal the effect of biomass pyrolysis vapors on the catalyst. Regenerated catalyst extrudates were obtained after calcining the spent extrudates at 250 °C for 40 min with a heating ramp of 4.5 °C·min^{-1} under a static air atmosphere followed by a second calcination at 600 °C for 5 h with a heating ramp of 5 °C·min^{-1} under an air atmosphere.[33] Spent and regenerated catalyst extrudates are further denoted following the *feedstock*-TOS and *feedstock*-TOSr sequences, respectively. The feedstock indicates the feed (either CELL or PW for cellulose and pinewood, respectively) used in catalytic pyrolysis tests, and TOS indicates the time-on-stream at which the sample is collected. For example, spent and regenerated extrudates obtained at TOS = 10 min from the CFP of cellulose and pine wood are represented as CELL-10 and CELL-10r and as PW-10 and PW-10r, respectively.

Catalytic Fast Pyrolysis Experiments. Catalytic Fast Pyrolysis (CFP) experiments were performed in a continuously operated fast pyrolysis system[34] employing auger reactor technology for the pyrolysis part and a fixed-bed reactor for the integrated *ex-situ* catalytic upgrading. *Ex situ* catalytic pyrolysis is preferred to avoid contact between biomass minerals (e.g., alkali and alkaline earth metals) and the catalyst particles,[35,36] thereby minimizing the contribution of minerals to the catalyst deactivation. The biomass (either pine wood or cellulose) was fed at a rate of ca. 0.2 kg h^{-1} while the catalyst bed contained 0.04 kg of catalyst. In this way a weight hourly space velocity (WHSV) of 5 h^{-1} on a feed basis was achieved. The temperature of the pyrolysis reactor and that of the catalytic reactor were kept at 500 °C during the experiments. CFP tests were performed at three different times-on-stream (TOS): 10, 60, and 180 min. The reactor scheme (Figure S7), with a detailed explanation of the experimental procedure and product analysis, is provided in the Supporting Information.

RESULTS AND DISCUSSION

Characterization of Fresh Catalysts. Textural properties of catalyst extrudates, such as porosity and crystallinity, are mainly dictated by the percentages of binder and active phase, and the preparation method used. Pore size distributions obtained after Hg porosimetry and Ar physisorption at −196 °C are shown in Figure 1a and b, respectively. In addition to HZSM-5 microporosity, alumina (Al_2O_3) mesopores were detected with a rather broad pore size distribution (up to 15 nm), confirming its highly amorphous nature. The technical HZSM-5/Al_2O_3 materials meso- and macroporosity (14 nm and ∼45 nm) are attributed to the Al_2O_3 and interparticle domain formation upon extrusion. These meso- and macropores can accommodate larger feedstock molecules.[37]

The physicochemical properties of the fresh extrudates are a weighted combination of the individual components (50:50), showing no major deviations. Figure 1c shows the FT-IR spectrum of the HZSM-5/Al_2O_3 catalyst extrudates (Figure 1c, see Table S1 for OH stretch assignments) shows similar vibrations as for the HZSM-5 and Al_2O_3 individual phases, revealing that no new sites were formed after extrusion.

The ^{27}Al solid state nuclear magnetic resonance (ss-NMR) spectra of zeolite, alumina, and the fresh composites (Figure

https://dx.doi.org/10.1021/acssuschemeng.0c07153
ACS Sustainable Chem. Eng. XXXX, XXX, XXX−XXX

1d) show that all individual contributions are present in the fresh HZSM-5/Al_2O_3 extrudates; i.e., no new aluminum sites are formed after extrusion. Two main peaks at 68 and 9 ppm are seen for the binder, corresponding to calcined and dehydrated boehmite-alumina.[38,39] Extra-framework octa- (0 ppm) and pentahedral (30 ppm) Al sites[40] and tetra-coordinated framework Brønsted acidic aluminum sites (55 ppm) are detected for the zeolite.[41−43]

Table 1 shows a summary of the physicochemical properties of the individual components and HZSM-5/Al_2O_3 catalyst extrudates. HZSM-5/Al_2O_3 showed a larger external surface area value than the HZSM-5 component after the addition of alumina, which may facilitate the condensation and/or cracking of large oligomeric species in pyrolysis vapors.

Table 1. Physicochemical Properties of the Individual Components and the Fresh HZSM-5/Al_2O_3 Catalyst Extrudates[a]

	HZSM-5	Al_2O_3	HZSM-5/Al_2O_3
S_{BET} (m^2 g^{-1} cat)	460	188	273
S_{micro} (m^2 g^{-1} cat)	405	-	166
S_{ext} (m^2 g^{-1} cat)	55	208	107
V_{micro} (cm^3 g^{-1} cat)	0.14	-	0.06
V_{meso} (cm^3 g^{-1} cat)	0.05	0.52	0.27
total amount of acid sites (μmol g^{-1} cat)	862	408	620 (635)
desorption temperature of strong acid sites (°C)	380	-	358
Lewis acid sites (μmol g^{-1} cat)	94	237	129 (165)
Brønsted acid sites (μmol g^{-1} cat)	144	-	79 (72)

[a]Between brackets, the theoretical acidity values calculated for an ideal 50:50 wt % mixture of zeolite and alumina are shown.

Acidity in the catalyst extrudates was evaluated by temperature-programmed desorption (TPD) of NH_3 (Figure S1b) and pyridine FT-IR spectroscopy and Brønsted and Lewis acidity calculated based on the latter[44] (see Table 1). HZSM-5/Al_2O_3 catalyst extrudates again showed a roughly additive contribution of acid sites from each individual component. In short, no dealumination was observed to occur during the synthesis-extrusion process of the catalyst extrudates. Expectedly, both individual components contain Lewis acid sites (LAS), while only the zeolite has Brønsted acid sites (BAS). Mixing and extrusion led to a slightly higher amount of both the Lewis and Brønsted acid sites in the HZSM-5/Al_2O_3 extrudates than expected, possibly because the higher external surface area enabled an improved accessibility and diffusion of the basic probe molecules. There is therefore no evidence indicating dealumination or neutralization of BAS by Al migration from the binder to the zeolite: the intrinsic acidity of the HZSM-5 component remained intact after extrusion. The contribution of additional LAS, introduced by the Al_2O_3 binder, is significant and needs to be taken into account in the catalytic activity studies (*vide infra*, see next section).

The morphology and distribution of the zeolite and alumina domains over the composite catalyst extrudates were analyzed by scanning electron microscopy−energy-dispersive X-ray (SEM-EDX; Figure S2),[28,45] using Si and Al signals to identify the zeolite alumina domains (which have a much higher Al content than the zeolite). Focused ion beam−scanning electron microscopy (FIB-SEM) experiments allowed the distribution of each phase within the catalyst extrudate to be visualized in detail (Figure 2). The SEM electron image (Figure 2a) reveals an irregular and dotted pattern which clearly corresponds to the zeolite (darker domains as they coincide with the Si-rich yellow parts) and alumina phases as indicated in the EDX images (Figure 2b).

Moreover, voids can be seen (~ 0.1 μm) that contribute to the macropore interparticle network between the zeolite and alumina agglomerates, as also suggested by Hg porosimetry.[18,37,46] However, even these relatively large-sized pore networks may not be large enough to accommodate the aerosols produced also upon pyrolysis of cellulose and lignin biopolymers. Indeed, the particle diameter of these aerosols is

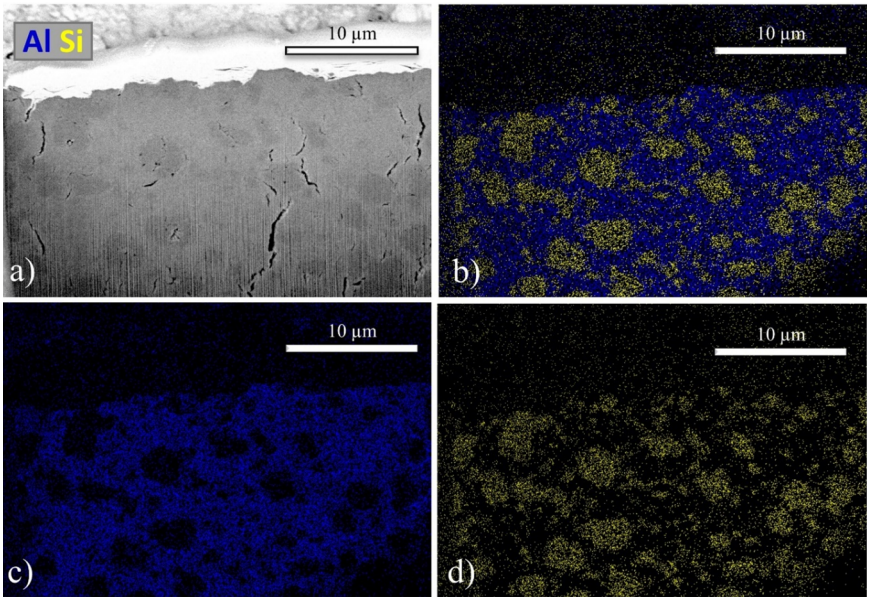

Figure 2. (a) Scanning electron microscopy (SEM) and energy-dispersive X-ray (EDX) images of (b) Al and Si, (c) Al, and (d) Si obtained after the focused ion beam (FIB) milling in the center of the cross section of a fresh HZSM-5/Al_2O_3 catalyst extrudate.

https://dx.doi.org/10.1021/acssuschemeng.0c07153
ACS Sustainable Chem. Eng. XXXX, XXX, XXX−XXX

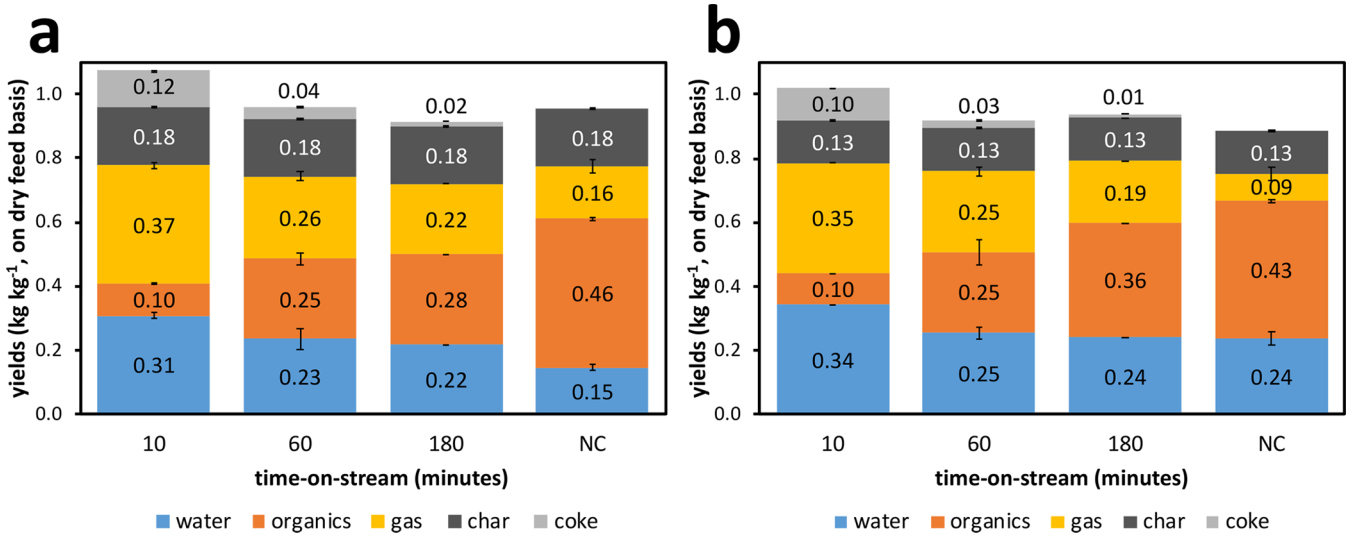

Figure 3. Product yields of catalytic pyrolysis of (a) pine wood and (b) cellulose obtained at the experimental conditions of $T_{pyrolysis}$ = 500 °C, $T_{catalysis}$ = 500 °C, and WHSV = 5.0 h^{-1}. Noncatalytic pyrolysis (NC) yields (run time = 60 min) for each feedstock are provided for comparison. Error bars represent standard deviation from the mean of duplicate experiments for all cases.

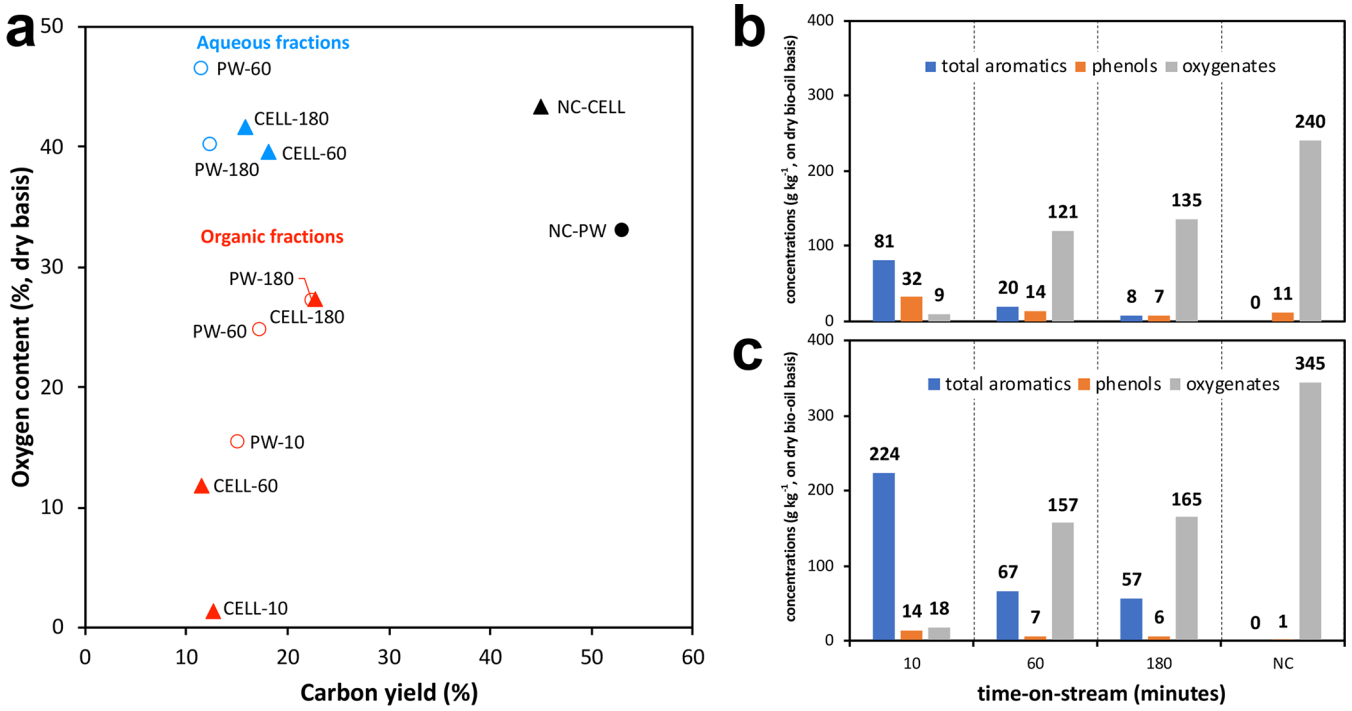

Figure 4. (a) Oxygen content (dry basis) and carbon yield of bio-oil fractions obtained upon *ex-situ* catalytic pyrolysis of pine wood and cellulose. Aqueous fractions at 10 min TOS are not included in the plot as they contain mostly water (>0.97 g g^{-1}). NC-PW (●) and NC-CELL (▲) values in the plot represent the noncatalytic pyrolysis yields of pine wood and cellulose, respectively. Conditions: $T_{pyrolysis}$ = 500 °C, $T_{catalytic}$ = 500 °C, WHSV = 5.0 h^{-1}. The composition of catalytic and noncatalytic bio-oils produced from (b) pine wood and (c) cellulose. Total aromatics = BTX and polycyclic aromatics (naphthalene, indene, and their substituted forms). Phenols = phenol and substituted phenols; oxygenates = acids, aldehydes, ketones, furans, and anhydrosugars.

reported to be between 0.5 and 10 μm, the majority of them being close to 1.0 μm.[47,48]

Catalytic Fast Pyrolysis Experiments. Catalytic fast pyrolysis (*ex situ*) of pine wood and cellulose using HZSM-5/Al_2O_3 extrudates as catalysts yielded char, noncondensable gas, bio-oil (water and condensable organics), and coke as products. The product yields, including those from a noncatalytic (NC) pyrolysis experiment as a reference, are summarized in Figure 3. At high catalyst-to-biomass ratios (i.e., low space velocities), the conversion of pyrolysis vapors to catalytic products is reportedly very high,[49,50] but such operating conditions prevent observing the long-term effects of the vapors on the catalyst materials.[51] We therefore chose a rather high space velocity (5.0 h^{-1}) to clearly see the effects of pyrolysis vapors on the catalyst as well as on the evolution of catalytic products with increasing TOS.

For both feedstock types the catalytic product distribution differed significantly from the one obtained from the

https://dx.doi.org/10.1021/acssuschemeng.0c07153
ACS Sustainable Chem. Eng. XXXX, XXX, XXX−XXX

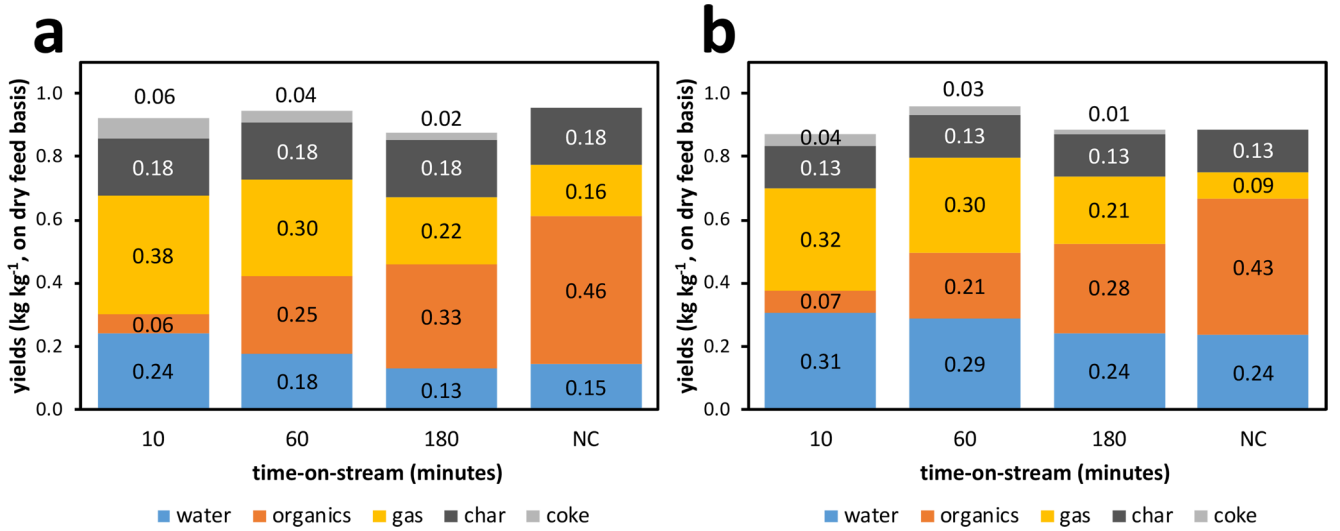

Figure 5. Product yields of catalytic fast pyrolysis (CFP) of (a) pine wood and (b) cellulose obtained with the regenerated catalysts at the experimental conditions of $T_{pyrolysis}$ = 500 °C, $T_{catalysis}$ = 500 °C, and WHSV = 5.0 h^{-1}. NC = Noncatalytic pyrolysis yields.

noncatalytic pyrolysis tests; it indicates a substantial catalytic activity of the HZSM-5/Al_2O_3. Overall, similar trends in product distribution were observed for pine wood and cellulose. The organic fractions produced upon pyrolysis are mostly converted to gas, water, and coke, especially at the shortest time-on-stream (i.e., highest catalyst/biomass ratio), in agreement with the literature.[6,27,52] Dehydration reactions are known to be the primary pathway of deoxygenation during catalytic pyrolysis of biomass,[53] particularly when using acidic zeolite ZSM-5-based catalysts. When the catalyst is at its most active state (10 min TOS), very similar water yields of 0.31 kg kg^{-1} and 0.34 kg kg^{-1} (on dry feed basis) are obtained for pine wood and cellulose, respectively. Correcting for thermally produced water during pyrolysis (see Figure 3 for the thermal (noncatalytic) water yields), the amounts of water produced at 10 min TOS by catalysis would be 0.16 kg kg^{-1} and 0.10 kg kg^{-1} for pine wood and cellulose, respectively. The hemicellulose and lignin fractions of pine wood thus considerably contribute to the observed catalytic dehydration, with the hemicellulose-derived vapors likely contributing the most. In addition to dehydration, decarbonylation and decarboxylation reactions also contribute to deoxygenation during biomass CFP. The formation of noncondensable gases (NCG), in particular CO and CO_2 (see Table S4), during the catalytic pyrolysis of pine wood seems to primarily originate from the reactions of the cellulose-derived vapors over the catalyst. This is evidenced by the substantial increase in the catalytic NCG yields of cellulose compared to the thermal (i.e., noncatalytic) NCG yields. In line with this, Wang et al.[21] showed that catalytic CO_x formation is more prominent for cellulose, if compared to lignin and hemicellulose. In terms of coke formation, a slightly higher fraction of feed intake is converted to coke with pine wood compared to cellulose. This slight increase may be attributed to lignin-derived vapors coking on the external surface of the catalyst.[22] With increasing TOS, the product distribution and the yields of individual product streams converge to the noncatalytic case, indicative of (partial) deactivation of the catalyst. However, the extent of the deactivation is not very severe. For instance, with the sample PW-180 (biomass-to-catalyst ratio of ~15), the noncatalytic biomass pyrolysis vapors seem to be still converted to gas and water. This is in contrast to the literature where HZSM-5 catalysts are reported to be completely deactivated at biomass-to-catalyst ratios of around 3 to 4, indicated by an increase in yields and oxygen contents of the catalytic liquids to the level of noncatalytic liquids.[10,54] The alumina binder could be causing this delay in deactivation by virtue of the introduced mesoporosity (see Table 1), similar to the hierarchical catalysts.[55,56] But with the current set of experiments, however, the reason behind this observation remains unknown.

The oxygen contents (on a dry basis) versus the carbon yields of the liquid product streams (aqueous and organic fractions), an important efficiency parameter,[9,57] are plotted in Figure 4a and highlight two shortcomings of the CFP process. First, the loss of C in the products of catalytic pyrolysis is obvious, if compared to the noncatalytic case, and for most cases not justified by the degree of deoxygenation levels obtained. Second, catalytic water production during CFP leads to phase separation in the bio-oil product resulting in aqueous and organic fractions. The aqueous fractions primarily contained water-soluble oxygenated pyrolysis products, while the organic fractions contained aromatic hydrocarbons and water-insoluble oxygenates. The phase separation in the bio-oil induced upon CFP will likely increase the downstream processing costs if both aqueous and organic streams are to be utilized. The valorization of the aqueous fractions will be of importance in particular at higher TOS (60 and 180 min), considering that the C yields in the aqueous and organic fractions are similar. The C yields of the aqueous phase of CFP liquids typically range from 3 to 14 wt % in the literature.[58] While the C yields of aqueous fractions reported here are at the higher end of that range, similarly high C yields (around 15 wt %) for aqueous fractions have been reported recently by Castello et al.[59] The compositions of catalytic and noncatalytic bio-oils were analyzed by GC/MS (Figures 4b and c) for both pine wood and cellulose. The total aromatics are the combined BTX and (substituted) polycyclic aromatic hydrocarbons (e.g., naphthalenes), while oxygenates are (non)catalytic products of biomass pyrolysis. It should be noted that (substituted) phenols can both be lignin-derived thermal products as well as result from the reaction of water and aromatic intermediates

https://dx.doi.org/10.1021/acssuschemeng.0c07153
ACS Sustainable Chem. Eng. XXXX, XXX, XXX−XXX

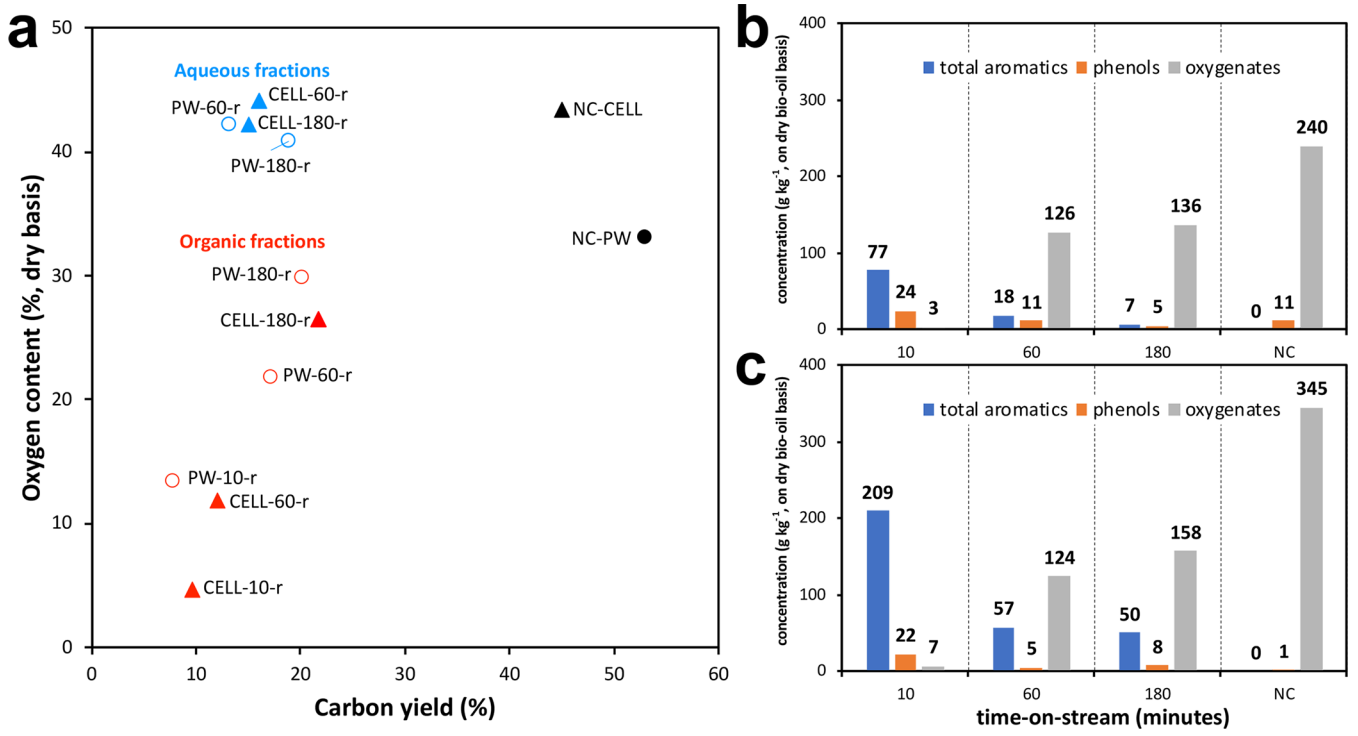

Figure 6. (a) Oxygen content (dry basis) and carbon yield of bio-oil fractions obtained upon ex-situ catalytic fast pyrolysis (CFP) of pine wood and cellulose with regenerated catalysts. Aqueous fractions at 10 min TOS are not included in the plot as they contain mostly water (>0.97 g g^{-1}). NC-PW (●) and NC-CELL (▲) values in the plot represent the noncatalytic pyrolysis yields of pine wood and cellulose, respectively. Conditions: $T_{pyrolysis}$ = 500 °C, $T_{catalytic}$ = 500 °C, WHSV = 5.0 h^{-1}. The composition of catalytic and noncatalytic bio-oils produced from (b) pine wood and (c) cellulose. Total aromatics include benzene, toluene, xylene, and polycyclic aromatics such as naphthalene, indene, and their substituted forms. Phenols include phenol and substituted phenols and the oxygenates include acids, aldehydes, ketones, furans, and anhydrosugars.

under biomass CFP conditions.[60] Lower aromatic hydrocarbon yields were obtained than reported in the literature, which may be attributed to the high WHSV employed in this work.[1,50,61] The precracking activity of the binder, by virtue of its Lewis acidity, cannot be neglected,[26,61−63] as demonstrated by py-GC/MS tests using a mixture of only the binder (Al_2O_3) and cellulose (see Figure S6). Given that only a limited fraction (<160 g kg^{-1} in case of pine wood) of the catalytic liquids could be quantified by GC/MS, it would be reasonable to assume that a significant fraction of the catalytic liquids is composed of high molecular weight components. This suggests that the precracking activity of the alumina binder seems to be limited under the process conditions investigated. On the other hand, the molar ratio of methane to light hydrocarbons (C 2s + C 3s; see Table S4) is still lower for PW-180 (1.8) than that of NC-PW (3.3), suggesting that there could still be some cracking going on even after 180 min time-on-stream. This form of cracking, however, could be ascribed to both the cleavage of propenyl structures from lignin-derived molecules and the cracking of cellulose-derived oxygenates. While the aromatic hydrocarbons (monoaromatics and polycyclic aromatics) dominate the liquid product chromatogram at a short time-on-stream, the composition of organics produced starts to resemble the noncatalytic cases with increasing TOS, again in line with (partial) deactivation of the catalyst. The selectivity toward aromatics production was found to be higher for cellulose than for pine. Compared to the noncatalytic results, a higher quality liquid product (i.e., lower oxygen content, more hydrocarbons) is obtained albeit at the expense of carbon yields; obviously a significant fraction of carbon in the feed is converted to coke and CO_x. While the loss of carbon through formation of CO_x is inevitable when the objective is to deoxygenate the pyrolysis vapors, loss through coke formation on the catalyst should be avoided and seems to be the primary obstacle for the CFP process. Because coke formation not only leads to the loss of feed C but also causes rapid catalyst deactivation, it increases the operating costs for the CFP process.

Catalytic Fast Pyrolysis Tests with Regenerated Catalysts. Catalytic pyrolysis activity after regeneration is shown in Figure 5, showing that organic product yields are lower with the regenerated catalysts (specifically at the shortest TOS). It should be noted that the mass balance closures are not as good as those obtained with the fresh catalysts (see Figure 3). The pine wood experiments indicate a clear decrease in dehydration activity at higher TOS, possibly due to the loss in acid sites following regeneration (see Figure 10). Additionally, lower coke yields were obtained which may be attributed directly to the slight decrease in Brønsted acid sites.

Overall, the carbon yield and oxygen content of the liquid products (Figure 6a) suggest that the loss of acid sites observed after one reaction/regeneration cycle does not affect the overall product composition drastically, however. In general, the trends observed with the fresh catalysts seem to prevail with the regenerated catalysts. The organic fractions obtained with the regenerated catalysts materials (shown in Figure 6b and c) contained 5−15% fewer aromatic hydrocarbons. Such a small decrease in aromatic hydrocarbons production upon catalyst regeneration is in line with previous reports.[33,64] The rapid deactivation and reduced performance already after one reaction/regeneration cycle suggest that a frequent addition of fresh makeup catalyst to the reactor would

https://dx.doi.org/10.1021/acssuschemeng.0c07153
ACS Sustainable Chem. Eng. XXXX, XXX, XXX−XXX

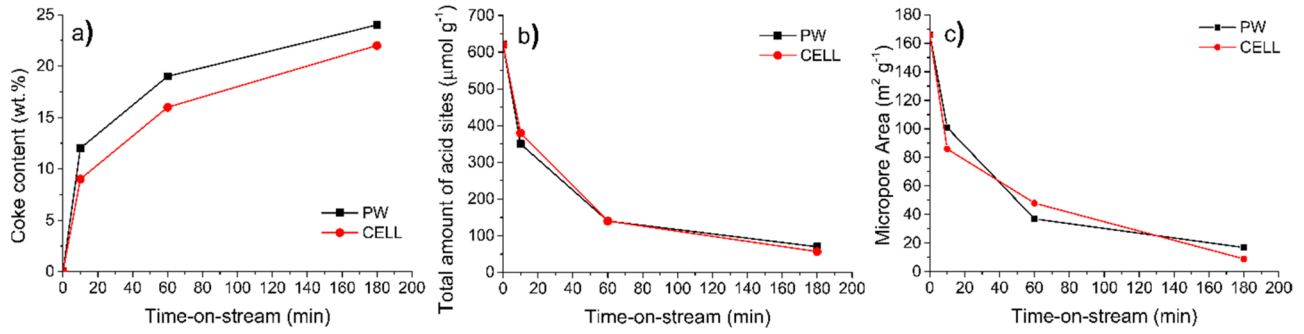

Figure 7. (a) Coke content, (b) total number of acid sites, and (c) micropore area from spent catalyst obtained at different time-on-stream (TOS) after catalytic fast pyrolysis (CFP) of pine wood (PW) and cellulose (CELL).

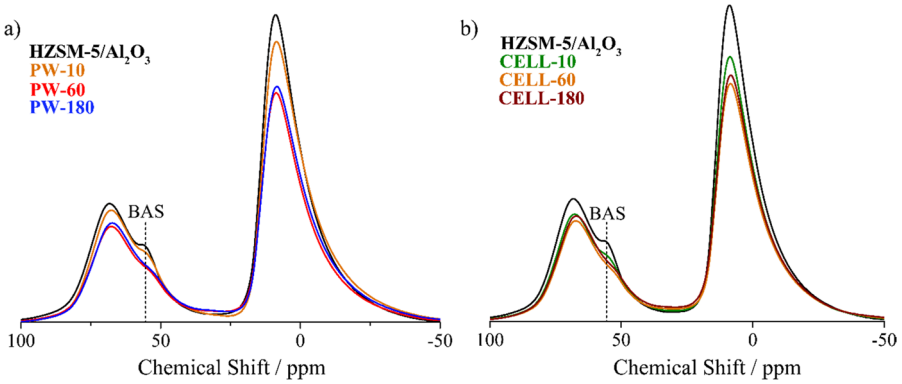

Figure 8. ^{27}Al solid state nuclear magnetic resonance (ss-NMR) spectra of (a) spent extrudates obtained after catalytic fast pyrolysis (CFP) of pine wood and (b) spent extrudates obtained after CFP of cellulose.

be required for long-term CFP operation. As shown in the previous sections, formation of carbon deposits on catalysts during CFP is directly correlated with the reaction conditions and feedstock used,[65] leading to a temporary deactivation of the catalyst materials. Regardless of regeneration, catalyst performance remains affected to a certain extent.[50,66]

Characterization of Spent Catalysts. Cellulose fast pyrolysis primarily produces levoglucosan and other small oxygenates (e.g., glycolaldehyde) in the bench-scale setup employed. The kinetic diameter of levoglucosan (0.67 nm) is reported to be slightly larger than the pore diameter of ZSM-5 (0.63 nm),[67] but levoglucosan may undergo dehydration reactions on the surface of the catalyst to produce smaller furan compounds which could easily diffuse into the pores of the catalyst.[21,68] In addition, hemicellulose-derived vapors would be composed of monomeric (anhydro)sugars and their defragmentation products, which can also diffuse easily into the pore network of the catalyst. However, the lignin-derived fraction of the vapors, which could correspond to up to 15% of pine wood vapors,[69] would next to phenolic monomers also contain oligomeric species. It is this relatively small fraction of oligomeric lignin species that could cause differences between the behavior of pine wood and cellulose vapors. While being larger than the pore diameters of the catalyst, these lignin oligomers will be condensed and/or cracked on the external surface of the catalyst.

Previous studies have demonstrated that an increase in coke contents correlates positively with a decrease of acidity and porosity.[70,71] In Figure 7, the coke content, the acidity, and the porosity of the spent extrudates are plotted as a function of TOS. Pine wood CFP leaves more coke on the spent catalyst extrudates. Independently of the quantity of coke formed for each feedstock, the decrease in the amount of acid sites occurs at a similar pace (Figure 7b). However, the micropores (Figure 7c) seems to be blocked faster with cellulose derived pyrolysis intermediates, in particular at the shortest TOS. While the coke content of the sample CELL-10 is ca. 30% lower than that of PW-10, a higher percentage of original micropore area is retained with the sample PW-10 (61% vs 52%). Additionally, the final values for the remaining micropore area and acid sites are lower in the CELL-180 than in the PW-180 (Table S2). Lignin-derived oligomers present in the pine wood vapors thus seem to block the external surface of the catalyst, restricting the access of small-sized (hemi)cellulose derived vapor phase compounds to the micropores. In contrast, during the CFP of cellulose, coke deposits appear to predominantly form in the zeolite micropores due to the unrestricted access of the small-sized cellulose-derived monomers, in line with recent observations.[22] Temperature Programmed Oxidation (TPO) analysis provided information on the carbonaceous deposits on and in the catalyst extrudates (Figure S3). At first glance, the MS profiles of all the samples display a similar pattern, revealing that the nature of coke does not depend on the type of feedstock (e.g., pine wood or cellulose) used, but only on the time on stream. As shown in other studies, CO_2 formation profiles may be used to determine the nature[10,72−77] or the location[56,72−74,78] of the coke in the catalyst. By monitoring CO_2 desorption profiles together with the H_2O desorption profiles, a more accurate estimation about the nature of the carbon deposits (e.g., soft or hard coke) can be obtained,[1,76] essential formation in order to determine the most efficient regeneration conditions (e.g., temperature, time). While soft coke species were observed in all spent samples, their share in overall coke species seemed to increase with increasing TOS as

https://dx.doi.org/10.1021/acssuschemeng.0c07153
ACS Sustainable Chem. Eng. XXXX, XXX, XXX−XXX

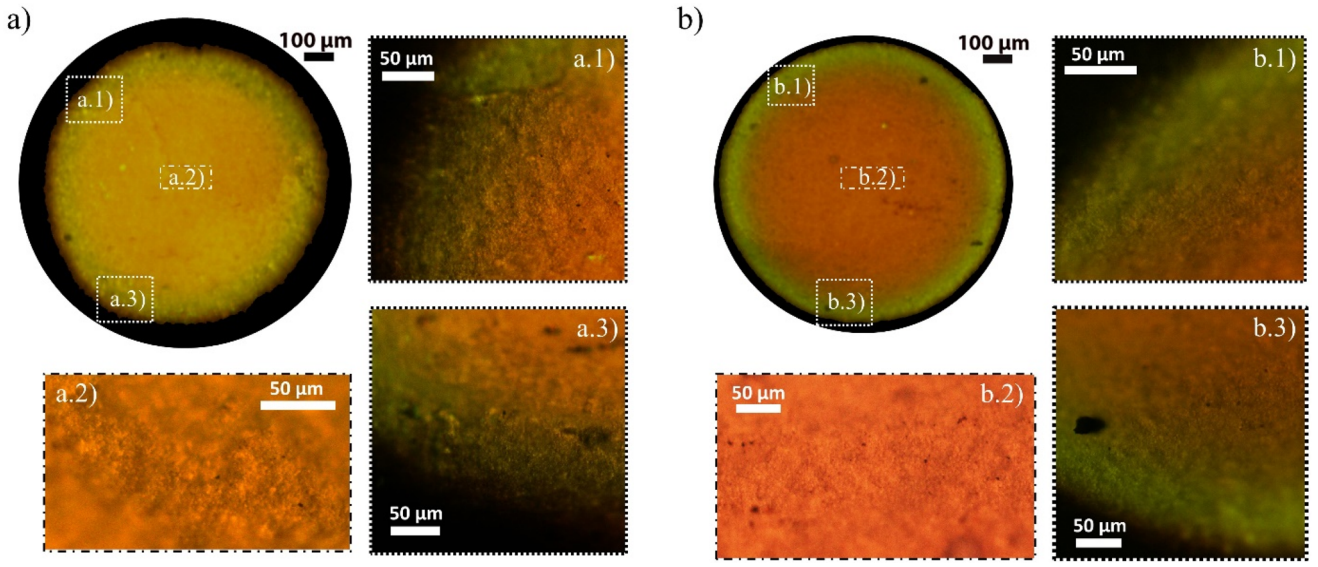

Figure 9. Confocal fluorescent microscopy (CFM) images obtained after irradiating the cross section of spent catalyst after 10 min time-on-stream (TOS) with 488 and 642 nm lasers after catalytic fast pyrolysis (CFP) of (a) pine wood (PW-10) and (b) cellulose (CELL-10).

previously noted.[31] Additionally, after curve fitting of the CO_2 desorption profiles, we could clearly distinguish three secondary desorption regions revealing information about the location of the coke species on and in the catalyst extrudates. These distinct CO_2 desorption regions showed that the coke species are present on the alumina binder (or on the external surface of the zeolite crystals),[74] at the pore mouth of the zeolite micropores[78] and on the catalytic sites of the micropores of the zeolites (see description in section 1.2 in Supporting Information). The intensities of these secondary CO_2 desorption regions suggest that, at higher TOS, the ratio between thermal coke and catalytic coke seems to increase. When catalysts remain for a longer time on stream, the amount of catalytic coke formed is limited because of a reduction in the number of active sites, as also observed by other authors.[56] At the same time, the quantity of thermal coke keeps increasing, even at the highest TOS, because its production is determined by noncatalytic condensation of oxygenated compounds. The formation of catalytic (hard) coke seems to start immediately upon the contact of pyrolysis vapors with the catalyst. The harsh, high T conditions required to remove such catalytic (hard) coke are expected to negatively affect the structure and the composition of the technical catalyst, for example leading to severe dealumination and dehydroxylation.[31,76]

The ss-NMR spectra of the spent samples showed a decrease in intensity and a notable broadening and shift toward lower chemical shifts above 50 ppm with increasing TOS (Figure 8a and b). As indicated by changes in the signal at 55 ppm, the loss of BAS is more substantial when using cellulose as the feedstock for pyrolysis. This observation is in accordance with the drop in micropore area shown in Figure 7c. This, together with the broadening and small shift to lower values of the 68 ppm peak, may be attributed to a structural change in the Al environment (poisoning and dealumination) caused by the formation of coke species.[79]

Confocal fluorescence microscopy (CFM, Figure S4a) provided insight into the spatial distribution of different carbon deposits over the extrudate.[80−82]

Fluorescence microscopy images of a cross section of PW-10 and CELL-10 spent catalyst materials and the corresponding magnifications are shown in Figure 9a and b. Almost no fluorescence was emitted from the cross-section of spent extrudates obtained at higher TOSs (i.e., 60 or 180 min), because of the higher concentration of condensed graphite-like coke species throughout the extrudate. Carbon deposits could be distinguished by size and nature[83,84] when illuminated with 488 and 642 nm lasers simultaneously, in the cross section of PW-10 and CELL-10 (Figure S4b and c). According to previous works,[18,85] the 488 nm laser only excites small aromatic species emitting green fluorescence (simple conjugated systems/rings; e.g., single aromatic carbocationic rings), while the 642 nm laser excites larger aromatic species emitting red fluorescence (≥2 aromatic carbocationic rings). Larger conjugated species (e.g., >3 aromatic rings) cannot be formed because the size of these species is much larger than the zeolite internal structure.[86,87]

For both spent extrudates a dense, nonfluorescent external layer of coke can be observed, corresponding to graphitic coke. Smaller coke species are detected over the cross-section for PW-10 than for CELL-10, with the latter also showing bigger aromatic carbon species in the core of the extrudate particle.

For both samples, when going from the edge to the center of the extrudate, a thin green layer followed by a pale orange domain located in the center can be discerned in Figure 9a, corresponding to a transition from a region where small conjugated species dominate (benzene- and/or naphthalene-like carbocations) to one where larger conjugated species do (naphthalene- and/or pyrene-like carbocations).[18] The more intense orange/red inner ring in CELL-10 (Figure 9b) indicates the higher concentration of larger carbocations compared to PW-10, suggesting that cellulose vapors diffuse more easily through the extrudate pores due to their smaller size. Eventually, these species react and form larger aromatics, becoming larger coke deposits. The thicker external layer of condensed coke seen for PW-10, again, suggests that the larger molecules in its vapors condense and oligomerize mostly at the external surface.[22]

According to the observations made by Whiting et al.,[18] molecules enter the catalyst pores and as they diffuse through the catalyst extrudate, they undergo cracking and oligomeriza-

https://dx.doi.org/10.1021/acssuschemeng.0c07153
ACS Sustainable Chem. Eng. XXXX, XXX, XXX−XXX

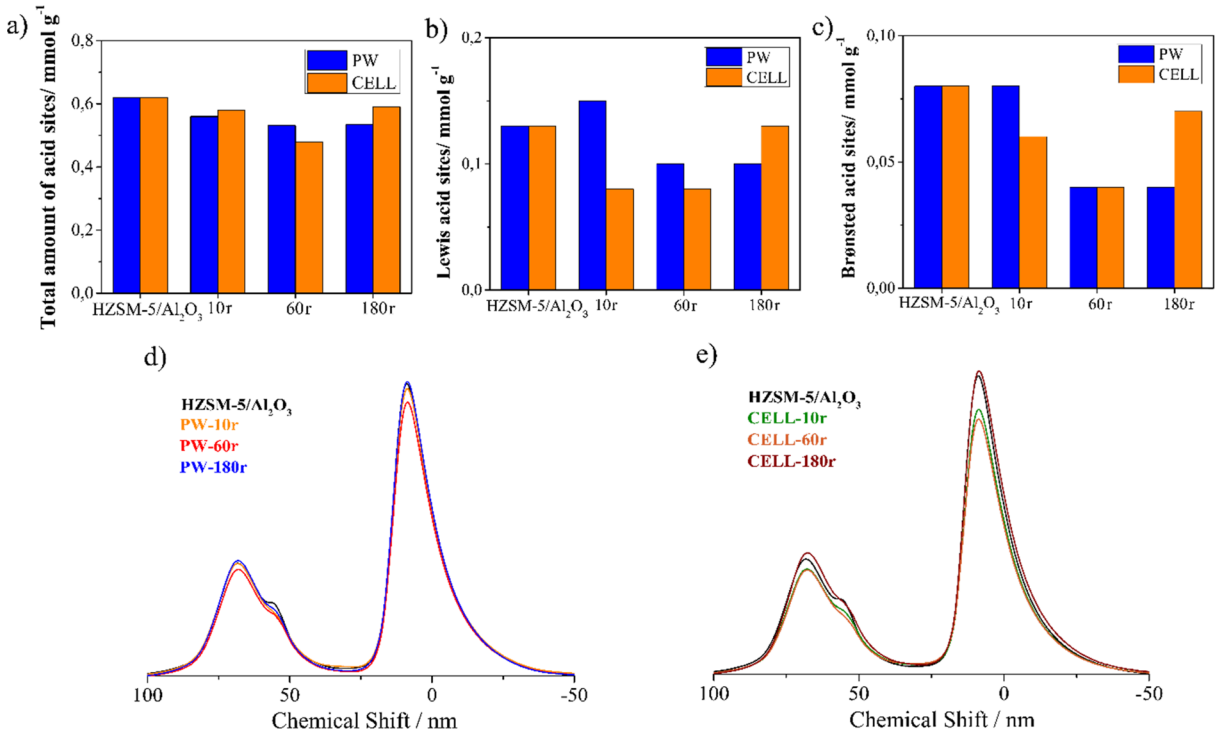

Figure 10. Total number of acid sites (a) of the regenerated extrudates was obtained by NH_3-TPD. (b) The total number of Lewis acid sites and (c) the total number of Brønsted acid sites available after regeneration were calculated after pyridine adsorption and FT-IR measurements. ^{27}Al ss-NMR spectra of the regenerated catalyst after one cycle for (d) the CFP of pine wood and (e) the CFP of cellulose.

tion reactions over time to form polyaromatic or conjugated species. If a transport barrier is present at a certain location inside the extrudate (e.g., pore narrowing), these enlarged species will be unable to diffuse out of the interior again. Instead, they will accumulate in the central part of the catalyst body. As shown in Figure S2, both zeolite and alumina domains are distributed evenly over the entire volume of the catalyst particle, suggesting that the intrinsic catalytic activity must be the same and comparable all along the catalyst extrudates. Diffusion limitations of the various pyrolysis vapors (size-dependent barrier) are therefore most likely the main reason for the observed circular fluorescent microscopy patterns. A possible and fast solution one can think of is the partial enlargement of the microporous structure to avoid mass transfer limitations. However, it is not an easy task as previous investigations on the incorporation of mesopores to MFI zeolites have revealed it to negatively affect aromatics selectivity, with the enlarged pore network leading to more coke formation instead.[55,56]

Characterization of Regenerated Catalysts. Regeneration of the spent catalysts by two-step calcination completely restored the textural properties of the catalysts used for pine wood CFP (Table S3), while some surface area loss was noted for spent cellulose CFP catalyst.

In Figure 10, the number and type of acid sites and the ^{27}Al ss-NMR spectra of the regenerated extrudates are shown.

NH_3-TPD and pyridine FT-IR analyses show that the total acidity could not be completely restored by the applied regeneration process, showing a slight drop in acidity for all samples (Figure 10a, b, and c). A more pronounced loss of Lewis acid sites (LAS) is seen for the regenerated CELL extrudates, as also evidenced by a decrease in intensity shown in the ss-NMR spectra for the Al (VI) sites at 0 ppm (Figure 10e). In contrast, for Brønsted acidity, a larger drop is observed for the CELL batch than for the PW batch at short TOS, likely as a result of partial restoration or partial dealumination of the zeolite. The NMR spectra of the regenerated extrudates still show a lower intensity for the peak at 55 ppm compared to the fresh extrudates. In the case of dealumination, it is noteworthy that the loss of catalyst acidity is dependent on (a) the type of pyrolysis feedstock (either being pine wood or cellulose) and (b) the time on stream during CFP.

The lower acidity values could be a cause of dealumination due to the high temperatures used during calcination, because coke deposits were reported to be efficiently removed from ZSM-5-based catalyst extrudates at calcination temperatures around 500 °C.[31] If dealumination is one of the causes, that will imply that acid sites are being lost as a result of the CFP process (500 °C) and of the regeneration process itself (600 °C). However, other authors reported that regeneration of catalysts consisting of ZSM-5 need at least calcination temperatures around 650 and 700 °C to fully restore porosity and acid sites after biomass CFP.[76] On the basis of our results, we believe that the lower acidity values obtained from our regenerated catalysts are most likely an indication that a partial regeneration has taken place instead of a partial dealumination, since our technical and shaped system is slightly more robust ($HZSM\text{-}5/Al_2O_3$) than pure ZSM-5 powder. Although, further experiments are required to confirm this hypothesis.

CONCLUSIONS

The performance of an Al_2O_3-bound ZSM-5-based technical catalyst has been assessed in the *ex situ* CFP of pine wood and cellulose. Postextrusion characterization of the technical catalyst indicated the effective dilution of the bulk zeolite's catalytic activity. However, the size of the meso- and

https://dx.doi.org/10.1021/acssuschemeng.0c07153
ACS Sustainable Chem. Eng. XXXX, XXX, XXX−XXX

macropore domains observed within the catalyst extrudates might be too small to accommodate the large aerosols ejected during pyrolysis of biomass. Catalytic pyrolysis product yields and composition converged to that of noncatalytic pyrolysis with increasing time-on-stream as a result of catalyst deactivation by coking. In agreement with previous reports, coking seems to be the primary challenge for the CFP process, leading to both a loss of carbon and catalyst deactivation. Interestingly, the Lewis acid sites of the alumina binder also exhibited catalytic activity, highlighting the importance of binder selection in future studies. Multitechnique characterization of spent catalysts showed subtle differences between pine wood and cellulose CFP, suggesting that the constituents of the lignocellulosic biomass coke differently. While small oxygenates (mostly derived from cellulose) form catalytic coke via ring-growth reactions inside the micropores of the catalyst, large oligomeric species (mostly derived from lignin) appear to form thermal coke on the binder and the external surface of the zeolite. The catalytic coke, known to be refractory to regeneration, starts to form immediately upon contact of the pyrolysis vapors with the catalyst. The thermal coke can be removed easily by regeneration; however, its presence blocks the access of small molecules to the active sites of the catalyst. Following catalyst regeneration, irreversible chemical changes in the catalyst structure (e.g., decrease in the aluminum content) were observed for both feedstock types, causing a loss of activity even after a single reaction/regeneration cycle. In conclusion, the feed-dependent interplay of mass transfer limitations and CFP chemistry appears to govern the CFP process. This complexity makes it very challenging to design a zeolite-based catalyst capable of efficiently converting biomass pyrolysis vapors to hydrocarbons.

■ ASSOCIATED CONTENT

Supporting Information

The Supporting Information is available free of charge at https://pubs.acs.org/doi/10.1021/acssuschemeng.0c07153.

Additional characterization of the catalysts prior to and after catalytic fast pyrolysis, including X-ray diffraction, Ar physisorption, temperature-programmed oxidation profiles, noncondensable gas compositions, py-GC/MS pyrograms, and a schematic illustration of the catalytic fast pyrolysis system used (PDF)

■ AUTHOR INFORMATION

Corresponding Authors

Bert M. Weckhuysen − *Inorganic Chemistry and Catalysis Group, Debye Institute for Nanomaterials Science, Utrecht University, 3584 CG Utrecht, The Netherlands;* orcid.org/0000-0001-5245-1426; Email: B.M.Weckhuysen@uu.nl

Mehmet Pala − *Thermochemical Conversion of Biomass Research Group, Department of Green Chemistry and Technology, Ghent University, 9000 Ghent, Belgium;* Email: Mehmet.Pala@UGent.be

Authors

Beatriz Luna-Murillo − *Inorganic Chemistry and Catalysis Group, Debye Institute for Nanomaterials Science, Utrecht University, 3584 CG Utrecht, The Netherlands*

Alessandra Lucini Paioni − *NMR Spectroscopy, Bijvoet Center for Biomolecular Research, Utrecht University, 3584 CH Utrecht, The Netherlands;* orcid.org/0000-0001-6609-6672

Marc Baldus − *NMR Spectroscopy, Bijvoet Center for Biomolecular Research, Utrecht University, 3584 CH Utrecht, The Netherlands;* orcid.org/0000-0001-7068-5613

Frederik Ronsse − *Thermochemical Conversion of Biomass Research Group, Department of Green Chemistry and Technology, Ghent University, 9000 Ghent, Belgium;* orcid.org/0000-0002-3290-9177

Wolter Prins − *Thermochemical Conversion of Biomass Research Group, Department of Green Chemistry and Technology, Ghent University, 9000 Ghent, Belgium*

Pieter C. A. Bruijnincx − *Inorganic Chemistry and Catalysis Group, Debye Institute for Nanomaterials Science and Organic Chemistry and Catalysis Group, Debye Institute for Nanomaterials Science, Utrecht University, 3584 CG Utrecht, The Netherlands*

Complete contact information is available at: https://pubs.acs.org/10.1021/acssuschemeng.0c07153

Author Contributions

#These authors contributed equally to this work.

Notes

The authors declare no competing financial interest.

■ ACKNOWLEDGMENTS

The authors thank Nikolaos Nikolopoulos (Utrecht University) for the (FIB)SEM-EDX measurements. This work was supported by The Netherlands Center for Multiscale Catalytic Energy Conversion (MCEC), an NWO Gravitation program funded by the Ministry of Education, Culture and Science of the government of The Netherlands and the SBO proposal "Bioleum: Fuels and chemicals by fast pyrolysis of biomass" (grant no: 130039) supported by the Institute for promotion of Innovation through Science and Technology in Flanders (IWT).

■ REFERENCES

(1) Carlson, T. R.; Cheng, Y.-T.; Jae, J.; Huber, G. W. Production of Green Aromatics and Olefins by Catalytic Fast Pyrolysis of Wood Sawdust. *Energy Environ. Sci.* **2011**, *4*, 145−161.

(2) Dickerson, T.; Soria, J. Catalytic Fast Pyrolysis: A Review. *Energies* **2013**, *6*, 514−538.

(3) Diebold, J.; Scahill, J. Biomass to Gasoline. *Pyrolysis Oils from Biomass* **1988**, *376*, 264.

(4) Williams, P. T.; Horne, P. A. The Influence of Catalyst Type on the Composition of Upgraded Biomass Pyrolysis Oils. *J. Anal. Appl. Pyrolysis* **1995**, *31*, 39−61.

(5) Carlson, T. R.; Jae, J.; Lin, Y. C.; Tompsett, G. A.; Huber, G. W. Catalytic Fast Pyrolysis of Glucose with HZSM-5: The Combined Homogeneous and Heterogeneous Reactions. *J. Catal.* **2010**, *270*, 110−124.

(6) Iisa, K.; French, R. J.; Orton, K. A.; Yung, M. M.; Johnson, D. K.; Ten Dam, J.; Watson, M. J.; Nimlos, M. R. In Situ and Ex Situ Catalytic Pyrolysis of Pine in a Bench-Scale Fluidized Bed Reactor System. *Energy Fuels* **2016**, *30*, 2144.

(7) Puertolas, B.; Veses, A.; Callen, M. S.; Mitchell, S.; Garcia, T.; Perez-Ramirez, J. Porosity-Acidity Interplay in Hierarchical ZSM-5 Zeolites for Pyrolysis Oil Valorization to Aromatics. *ChemSusChem* **2015**, *8*, 3283−3293.

(8) Lee, H. W.; Park, S. H.; Jeon, J. K.; Ryoo, R.; Kim, W.; Suh, D. J.; Park, Y. K. Upgrading of Bio-Oil Derived from Biomass Constituents

over Hierarchical Unilamellar Mesoporous MFI Nanosheets. *Catal. Today* **2014**, *232*, 119−126.
(9) Venderbosch, R. H. A Critical View on Catalytic Pyrolysis of Biomass. *ChemSusChem* **2015**, *8* (8), 1306−1316.
(10) Mukarakate, C.; Zhang, X.; Stanton, A. R.; Robichaud, D. J.; Ciesielski, P. N.; Malhotra, K.; Donohoe, B. S.; Gjersing, E.; Evans, R. J.; Heroux, D. S.; Richards, R.; Iisa, K.; Nimlos, M. R. Real-Time Monitoring of the Deactivation of HZSM-5 during Upgrading of Pine Pyrolysis Vapors. *Green Chem.* **2014**, *16* (3), 1444−1461.
(11) CHANG, C The Conversion of Methanol and Other O-Compounds to Hydrocarbons over Zeolite Catalysts. *J. Catal.* **1977**, *47*, 249−259.
(12) Chantal, P.; Kaliaguine, S.; Grandmaison, J.-L.; Mahay, A. Production of Hydrocarbons from Aspen Poplar Pyrolytic Oils Over H-ZSM5. *Appl. Catal.* **1984**, *10*, 317−332.
(13) Stöcker, M. Methanol-to-Hydrocarbons: Catalytic Materials and Their Behavior. *Microporous Mesoporous Mater.* **1999**, *29* (1−2), 3−48.
(14) Park, H. J.; Heo, H. S.; Jeon, J. K.; Kim, J.; Ryoo, R.; Jeong, K. E.; Park, Y. K. Highly Valuable Chemicals Production from Catalytic Upgrading of Radiata Pine Sawdust-Derived Pyrolytic Vapors over Mesoporous MFI Zeolites. *Appl. Catal., B* **2010**, *95* (3−4), 365−373.
(15) Carlson, T. R.; Jae, J.; Huber, G. W. Mechanistic Insights from Isotopic Studies of Glucose Conversion to Aromatics over ZSM-5. *ChemCatChem* **2009**, *1* (1), 107−110.
(16) Kelkar, S.; Saffron, C. M.; Andreassi, K.; Li, Z.; Murkute, A.; Miller, D. J.; Pinnavaia, T. J.; Kriegel, R. M. A Survey of Catalysts for Aromatics from Fast Pyrolysis of Biomass. *Appl. Catal., B* **2015**, *174*−*175*, 85−95.
(17) Yarulina, I.; Chowdhury, A. D.; Meirer, F.; Weckhuysen, B. M.; Gascon, J. Recent Trends and Fundamental Insights in the Methanol-to-Hydrocarbons Process. *Nat. Catal.* **2018**, *1* (6), 398−411.
(18) Whiting, G. T.; Nikolopoulos, N.; Nikolopoulos, I.; Chowdhury, A. D.; Weckhuysen, B. M. Visualizing Pore Architecture and Molecular Transport Boundaries in Catalyst Bodies with Fluorescent Nanoprobes. *Nat. Chem.* **2019**, *11* (1), 23−31.
(19) Müller, S.; Liu, Y.; Vishnuvarthan, M.; Sun, X.; Van Veen, A. C.; Haller, G. L.; Sanchez-Sanchez, M.; Lercher, J. A. Coke Formation and Deactivation Pathways on H-ZSM-5 in the Conversion of Methanol to Olefins. *J. Catal.* **2015**, *325*, 48−59.
(20) Yu, Y.; Li, X.; Su, L.; Zhang, Y.; Wang, Y.; Zhang, H. The Role of Shape Selectivity in Catalytic Fast Pyrolysis of Lignin with Zeolite Catalysts. *Appl. Catal., A* **2012**, *447*−*448*, 115−123.
(21) Wang, K.; Kim, K. H.; Brown, R. C. Catalytic Pyrolysis of Individual Components of Lignocellulosic Biomass. *Green Chem.* **2014**, *16*, 727−735.
(22) Stanton, A. R.; Iisa, K.; Mukarakate, C.; Nimlos, M. R. Role of Biopolymers in the Deactivation of ZSM-5 during Catalytic Fast Pyrolysis of Biomass. *ACS Sustainable Chem. Eng.* **2018**, *6* (8), 10030−10038.
(23) Wan, S.; Waters, C.; Stevens, A.; Gumidyala, A.; Jentoft, R.; Lobban, L.; Resasco, D.; Mallinson, R.; Crossley, S. Decoupling HZSM-5 Catalyst Activity from Deactivation during Upgrading of Pyrolysis Oil Vapors. *ChemSusChem* **2015**, *8* (3), 552−559.
(24) Mitchell, S.; Michels, N.-L.; Perez-Ramirez, J. From Powder to Technical Body: The Undervalued Science of Catalyst Scale Up. *Chem. Soc. Rev.* **2013**, *42* (14), 6094.
(25) Vogt, E. T. C.; Weckhuysen, B. M. Fluid Catalytic Cracking: Recent Developments on the Grand Old Lady of Zeolite Catalysis. *Chem. Soc. Rev.* **2015**, *44* (20), 7342−7370.
(26) Zhang, H.; Xiao, R.; Jin, B.; Xiao, G.; Chen, R. Biomass Catalytic Pyrolysis to Produce Olefins and Aromatics with a Physically Mixed Catalyst. *Bioresour. Technol.* **2013**, *140*, 256−262.
(27) Mante, O. D.; Dayton, D. C.; Carpenter, J. R.; Wang, K.; Peters, J. E. Pilot-Scale Catalytic Fast Pyrolysis of Loblolly Pine over Γ-Al2O3catalyst. *Fuel* **2018**, *214*, 569−579.
(28) Whiting, G. T.; Meirer, F.; Mertens, M. M.; Bons, A. J.; Weiss, B. M.; Stevens, P. A.; De Smit, E.; Weckhuysen, B. M. Binder Effects in SiO2- and Al2O3-Bound Zeolite ZSM-5-Based Extrudates as Studied by Microspectroscopy. *ChemCatChem* **2015**, *7* (8), 1312−1321.
(29) Ruiz-Martínez, J.; Buurmans, I. L. C.; Knowles, W. V.; Van Der Beek, D.; Bergwerff, J. A.; Vogt, E. T. C.; Weckhuysen, B. M. Microspectroscopic Insight into the Deactivation Process of Individual Cracking Catalyst Particles with Basic Sulfur Components. *Appl. Catal., A* **2012**, *419*−*420*, 84−94.
(30) De Winter, D. A. M.; Meirer, F.; Weckhuysen, B. M. FIB-SEM Tomography Probes the Mesoscale Pore Space of an Individual Catalytic Cracking Particle. *ACS Catal.* **2016**, *6* (5), 3158−3167.
(31) Heracleous, E.; Pachatouridou, E.; Hernández-Giménez, A. M.; Hernando, H.; Fakin, T.; Paioni, A. L.; Baldus, M.; Serrano, D. P.; Bruijnincx, P. C. A.; Weckhuysen, B. M.; Lappas, A. A. Characterization of Deactivated and Regenerated Zeolite ZSM-5-Based Catalyst Extrudates Used in Catalytic Pyrolysis of Biomass. *J. Catal.* **2019**, *380*, 108−122.
(32) Hernando, H.; Hernández-Giménez, A. M.; Gutiérrez-Rubio, S.; Fakin, T.; Horvat, A.; Danisi, R. M.; Pizarro, P.; Fermoso, J.; Heracleous, E.; Bruijnincx, P. C. A.; Lappas, A. A.; Weckhuysen, B. M.; Serrano, D. P. Scaling-Up of Bio-Oil Upgrading during Biomass Pyrolysis over ZrO2/ZSM-5-Attapulgite. *ChemSusChem* **2019**, *12*, 2428−2438.
(33) Yildiz, G.; Lathouwers, T.; Toraman, H. E.; van Geem, K. M.; Marin, G. B.; Ronsse, F.; van Duren, R.; Kersten, S. R. A.; Prins, W. Catalytic Fast Pyrolysis of Pine Wood: Effect of Successive Catalyst Regeneration. *Energy Fuels* **2014**, *28*, 4560−4572.
(34) Yildiz, G.; Pronk, M.; Djokic, M.; Van Geem, K. M.; Ronsse, F.; Van Duren, R.; Prins, W. Validation of a New Set-up for Continuous Catalytic Fast Pyrolysis of Biomass Coupled with Vapour Phase Upgrading. *J. Anal. Appl. Pyrolysis* **2013**, *103*, 343−351.
(35) Yildiz, G.; Ronsse, F.; Venderbosch, R.; Duren, R.; van Kersten, S. R. A.; Prins, W. Effect of Biomass Ash in Catalytic Fast Pyrolysis of Pine Wood. *Appl. Catal., B* **2015**, *168*−*169*, 203−211.
(36) Yung, M. M.; Stanton, A. R.; Iisa, K.; French, R. J.; Orton, K. A.; Magrini, K. A. Multiscale Evaluation of Catalytic Upgrading of Biomass Pyrolysis Vapors on Ni- and Ga-Modified ZSM-5. *Energy Fuels* **2016**, *30* (11), 9471−9479.
(37) Michels, N. L.; Mitchell, S.; Pérez-Ramírez, J. Effects of Binders on the Performance of Shaped Hierarchical MFI Zeolites in Methanol-to-Hydrocarbons. *ACS Catal.* **2014**, *4* (8), 2409−2417.
(38) Samain, L.; Jaworski, A.; Edén, M.; Ladd, D. M.; Seo, D. K.; Javier Garcia-Garcia, F.; Häussermann, U. Structural Analysis of Highly Porous γ-Al2O3. *J. Solid State Chem.* **2014**, *217*, 1−8.
(39) Paglia, G.; Buckley, C. E.; Rohl, A. L.; Hart, R. D.; Winter, K.; Studer, A. J.; Hunter, B. A.; Hanna, J. V. Boehmite Derived γ-Alumina System. 1. Structural Evolution with Temperature, with the Identification and Structural Determination of a New Transition Phase, Γ′-Alumina. *Chem. Mater.* **2004**, *16* (2), 220−236.
(40) Jiang, Y.; Huang, J.; Dai, W.; Hunger, M. Solid-State Nuclear Magnetic Resonance Investigations of the Nature, Property, and Activity of Acid Sites on Solid Catalysts. *Solid State Nucl. Magn. Reson.* **2011**, *39* (3−4), 116−141.
(41) Klinowski, J. Nuclear Magnetic Resonance Studies of Zeolites. *Prog. Nucl. Magn. Reson. Spectrosc.* **1984**, *16*, 237−309.
(42) Samoson, A.; Lippmaa, E.; Engelhardt, G.; Lohse, U.; Jerschkewitz, H. G. Quantitative High-Resolution 27Al NMR: Tetrahedral Non-Framework Aluminium in Hydrothermally Treated Zeolites. *Chem. Phys. Lett.* **1987**, *134* (6), 589−592.
(43) Wang, Z.; Jiang, Y.; Lafon, O.; Trébosc, J.; Duk Kim, K.; Stampfl, C.; Baiker, A.; Amoureux, J. P.; Huang, J. Brønsted Acid Sites Based on Penta-Coordinated Aluminum Species. *Nat. Commun.* **2016**, *7*, 1−5.
(44) Thibault-Staruk, F.; Francoise, M. Part One Molecular/Local Spectroscopies. *Characterization of Solid Materials and Heterogeneous Catalysts* **2012**, 1−48.
(45) Verkleij, S. P.; Whiting, G. T.; Esclapez, S. P.; Mertens, M. M.; Bons, A.-J.; Burgers, M.; Weckhuysen, B. M. *Operando* Micro-Spectroscopy on ZSM-5 Containing Extrudates during the Oligomerization of 1-Hexene. *Catal. Sci. Technol.* **2018**, *8*, 2175−2185.

https://dx.doi.org/10.1021/acssuschemeng.0c07153
ACS Sustainable Chem. Eng. XXXX, XXX, XXX−XXX

(46) Mitchell, S.; Michels, N. L.; Kunze, K.; Pérez-Ramírez, J. Visualization of Hierarchically Structured Zeolite Bodies from Macro to Nano Length Scales. *Nat. Chem.* **2012**, *4* (10), 825−831.
(47) Teixeira, A. R.; Mooney, K. G.; Kruger, J. S.; Williams, C. L.; Suszynski, W. J.; Schmidt, L. D.; Schmidt, D. P.; Dauenhauer, P. J. Aerosol Generation by Reactive Boiling Ejection of Molten Cellulose. *Energy Environ. Sci.* **2011**, *4* (10), 4306.
(48) Montoya, J.; Pecha, B.; Janna, F. C.; Garcia-Perez, M. Micro-Explosion of Liquid Intermediates during the Fast Pyrolysis of Sucrose and Organosolv Lignin. *J. Anal. Appl. Pyrolysis* **2016**, *122*, 106−121.
(49) Aho, A.; Tokarev, A.; Backman, P.; Kumar, N.; Eranen, K.; Hupa, M.; Holmbom, B.; Salmi, T.; Murzin, D. Y. Catalytic Pyrolysis of Pine Biomass over H-Beta Zeolite in a Dual-Fluidized Bed Reactor: Effect of Space Velocity on the Yield and Composition of Pyrolysis Products. *Top. Catal.* **2011**, *54* (13−15), 941−948.
(50) Yang, H.; Coolman, R.; Karanjkar, P.; Wang, H.; Dornath, P.; Chen, H.; Fan, W.; Conner, W. C.; Mountziaris, T. J.; Huber, G. The Effects of Contact Time and Coking on the Catalytic Fast Pyrolysis of Cellulose. *Green Chem.* **2017**, *19* (1), 286−297.
(51) Kramm, U. I.; Marschall, R.; Rose, M. Pitfalls in Heterogeneous Thermal, Electro- and Photocatalysis. *ChemCatChem* **2019**, *11* (11), 2563−2574.
(52) Paasikallio, V.; Agblevor, F.; Oasmaa, A.; Lehto, J.; Lehtonen, J. Catalytic Pyrolysis of Forest Thinnings with ZSM-5 Catalysts: Effect of Reaction Temperature on Bio-Oil Physical Properties and Chemical Composition. *Energy Fuels* **2013**, *27*, 7587−7601.
(53) Hernando, H.; Jiménez-Sánchez, S.; Fermoso, J.; Pizarro, P.; Coronado, J. M.; Serrano, D. P. Assessing Biomass Catalytic Pyrolysis in Terms of Deoxygenation Pathways and Energy Yields for the Efficient Production of Advanced Biofuels. *Catal. Sci. Technol.* **2016**, *6*, 2829−2843.
(54) Zacher, A.; et al. Mild Catalytic Fast Pyrolysis of Biomass & Catalytic Hydrotreating to Liquid Transportation Fuels. In *TC Biomass 2011*; GTI, 2011.
(55) Xu, M.; Mukarakate, C.; Iisa, K.; Budhi, S.; Menart, M.; Davidson, M.; Robichaud, D. J.; Nimlos, M. R.; Trewyn, B. G.; Richards, R. M. Deactivation of Multilayered MFI Nanosheet Zeolite during Upgrading of Biomass Pyrolysis Vapors. *ACS Sustainable Chem. Eng.* **2017**, *5* (6), 5477−5484.
(56) Jia, L. Y.; Raad, M.; Hamieh, S.; Toufaily, J.; Hamieh, T.; Bettahar, M. M.; Mauviel, G.; Tarrighi, M.; Pinard, L.; Dufour, A. Catalytic Fast Pyrolysis of Biomass: Superior Selectivity of Hierarchical Zeolites to Aromatics. *Green Chem.* **2017**, *19* (22), 5442−5459.
(57) Saraeian, A.; Nolte, M. W.; Shanks, B. H. Deoxygenation of Biomass Pyrolysis Vapors: Improving Clarity on the Fate of Carbon. *Renewable Sustainable Energy Rev.* **2019**, *104*, 262−280.
(58) Starace, A. K.; Black, B. A.; Lee, D. D.; Palmiotti, E. C.; Orton, K. A.; Michener, W. E.; Ten Dam, J.; Watson, M. J.; Beckham, G. T.; Magrini, K. A.; Mukarakate, C. Characterization and Catalytic Upgrading of Aqueous Stream Carbon from Catalytic Fast Pyrolysis of Biomass. *ACS Sustainable Chem. Eng.* **2017**, *5* (12), 11761−11769.
(59) Castello, D.; He, S.; Ruiz, M. P.; Westerhof, R. J. M.; Heeres, H. J.; Seshan, K.; Kersten, S. R. A. Is It Possible to Increase the Oil Yield of Catalytic Pyrolysis of Biomass? A Study Using Commercially-Available Acid and Basic Catalysts in Ex-Situ and in-Situ Modus. *J. Anal. Appl. Pyrolysis* **2019**, *137*, 77.
(60) Mukarakate, C.; Mcbrayer, J. D.; Evans, T. J.; Budhi, S.; Robichaud, D. J.; Iisa, K.; Ten Dam, J.; Watson, M. J.; Baldwin, R. M.; Nimlos, M. R. Catalytic Fast Pyrolysis of Biomass: The Reactions of Water and Aromatic Intermediates Produces Phenols. *Green Chem.* **2015**, *17* (8), 4217−4227.
(61) Iisa, K.; French, R. J.; Orton, K. A.; Budhi, S.; Mukarakate, C.; Stanton, A. R.; Yung, M. M.; Nimlos, M. R. Catalytic Pyrolysis of Pine over HZSM-5 with Different Binders. *Top. Catal.* **2016**, *59* (1), 94−108.
(62) Hargreaves, J. S. J.; Munnoch, A. L. A Survey of the Influence of Binders in Zeolite Catalysis. *Catal. Sci. Technol.* **2013**, *3* (3), 1165−1171.
(63) Vogt, E. T. C.; Whiting, G. T.; Dutta Chowdhury, A.; Weckhuysen, B. M. *Zeolites and Zeotypes for Oil and Gas Conversion*, 1st ed.; Elsevier Inc., 2015; Vol. *58*. DOI: 10.1016/bs.a-cat.2015.10.001.
(64) Williams, P. T.; Horne, P. A. The Influence of Catalyst Regeneration on the Composition of Zeolite-Upgraded Biomass Pyrolysis Oils. *Fuel* **1995**, *74* (12), 1839−1851.
(65) Gayubo, A. G.; Aguayo, A. T.; Atutxa, A.; Valle, B.; Bilbao, J. Undesired Components in the Transformation of Biomass Pyrolysis Oil into Hydrocarbons on an HZSM-5 Zeolite Catalyst. *J. Chem. Technol. Biotechnol.* **2005**, *80* (11), 1244−1251.
(66) Cerqueira, H. S.; Caeiro, G.; Costa, L.; Ramoa Ribeiro, F. Deactivation of FCC Catalysts. *J. Mol. Catal. A: Chem.* **2008**, *292* (1−2), 1−13.
(67) Jae, J.; Tompsett, G. A.; Foster, A. J.; Hammond, K. D.; Auerbach, S. M.; Lobo, R. F.; Huber, G. W. Investigation into the Shape Selectivity of Zeolite Catalysts for Biomass Conversion. *J. Catal.* **2011**, *279* (2), 257−268.
(68) Wang, K.; Zhang, J. H.; Shanks, B.; Brown, R. C. Catalytic Conversion of Carbohydrate-Derived Oxygenates over HZSM-5 in a Tandem Micro-Reactor System. *Green Chem.* **2015**, *17* (1), 557−564.
(69) Oasmaa, A.; Solantausta, Y.; Arpiainen, V.; Kuoppala, E.; Sipilä, K. Fast Pyrolysis Bio-Oils from Wood and Agricultural Residues. *Energy Fuels* **2010**, *24* (2), 1380−1388.
(70) Gou, J.; Wang, Z.; Li, C.; Qi, X.; Vattipalli, V.; Cheng, Y.-T.; Conner, W. C.; Dauenhauer, P. J.; Mountziaris, T. J.; Fan, W.; Huber, G. The Effect of ZSM-5 Mesoporotsity and Morphology on the Catalytic Fast Pyrolysis of Furan. *Green Chem.* **2017**, *19*, 3549.
(71) Du, S.; Gamliel, D. P.; Giotto, M. V.; Valla, J. A.; Bollas, G. M. Coke Formation of Model Compounds Relevant to Pyrolysis Bio-Oil over ZSM-5. *Appl. Catal., A* **2016**, *513*, 67−81.
(72) Guisnet, M.; Magnoux, P. Organic Chemistry of Coke Formation. *Appl. Catal., A* **2001**, *212* (1−2), 83−96.
(73) Valle, B.; Castaño, P.; Olazar, M.; Bilbao, J.; Gayubo, A. G. Deactivating Species in the Transformation of Crude Bio-Oil with Methanol into Hydrocarbons on a HZSM-5 Catalyst. *J. Catal.* **2012**, *285* (1), 304−314.
(74) Du, S.; Valla, J. A.; Bollas, G. M. Characteristics and Origin of Char and Coke from Fast and Slow, Catalytic and Thermal Pyrolysis of Biomass and Relevant Model Compounds. *Green Chem.* **2013**, *15*, 3214.
(75) Liu, Y.; Kirchberger, F. M.; Müller, S.; Eder, M.; Tonigold, M.; Sanchez-Sanchez, M.; Lercher, J. A. Critical Role of Formaldehyde during Methanol Conversion to Hydrocarbons. *Nat. Commun.* **2019**, *10* (1), 1−9.
(76) Yung, M. M.; Starace, A. K.; Griffin, M. B.; Wells, J. D.; Patalano, R. E.; Smith, K. R.; Schaidle, J. A. Restoring ZSM-5 Performance for Catalytic Fast Pyrolysis of Biomass: Effect of Regeneration Temperature. *Catal. Today* **2019**, *323*, 76−85.
(77) Ibarra, Á.; Veloso, A.; Bilbao, J.; Arandes, J. M.; Castaño, P. Dual Coke Deactivation Pathways during the Catalytic Cracking of Raw Bio-Oil and Vacuum Gasoil in FCC Conditions. *Appl. Catal., B* **2016**, *182*, 336−346.
(78) Xian, X.; Ran, C.; Nai, C.; Yang, P.; Zhao, S.; Dong, L. Characterization of the Location of Coke Deposited on Spent HZSM-5 Zeolite by Special Temperature-Programmed Oxidation and Isothermal Oxidation Methods. *Appl. Catal., A* **2017**, *547*, 37−51.
(79) Devaraj, A.; Vijayakumar, M.; Bao, J.; Guo, M. F.; Derewinski, M. A.; Xu, Z.; Gray, M. J.; Prodinger, S.; Ramasamy, K. K. Discerning the Location and Nature of Coke Deposition from Surface to Bulk of Spent Zeolite Catalysts. *Sci. Rep.* **2016**, *6*, 1−11.
(80) Kox, M. H. F.; Stavitski, E.; Groen, J. C. C.; Pérez-Ramírez, J.; Kapteijn, F.; Weckhuysen, B. M. Visualizing the Crystal Structure and Locating the Catalytic Activity of Micro- and Mesoporous ZSM-5 Zeolite Crystals by Using In Situ Optical and Fluorescence Microscopy. *Chem. - Eur. J.* **2008**, *14* (6), 1718−1725.

https://dx.doi.org/10.1021/acssuschemeng.0c07153
ACS Sustainable Chem. Eng. XXXX, XXX, XXX−XXX

(81) Aramburo, L. R.; Karwacki, L.; Cubillas, P.; Asahina, S.; De Winter, D. A. M.; Drury, M. R.; Buurmans, I. L. C.; Stavitski, E.; Mores, D.; Daturi, M.; Bazin, P.; Dumas, P.; Thibault-Starzyk, F.; Post, J. A.; Anderson, M. W.; Terasaki, O.; Weckhuysen, B. M. The Porosity, Acidity, and Reactivity of Dealuminated Zeolite ZSM-5 at the Single Particle Level: The Influence of the Zeolite Architecture. *Chem. - Eur. J.* **2011**, *17* (49), 13773−13781.
(82) Ristanović, Z.; Kerssens, M. M.; Kubarev, A. V.; Hendriks, F. C.; Dedecker, P.; Hofkens, J.; Roeffaers, M. B. J.; Weckhuysen, B. M. High-Resolution Single-Molecule Fluorescence Imaging of Zeolite Aggregates within Real-Life Fluid Catalytic Cracking Particles. *Angew. Chem., Int. Ed.* **2015**, *54* (6), 1836−1840.
(83) Nordvang, E. C.; Borodina, E.; Ruiz-Martínez, J.; Fehrmann, R.; Weckhuysen, B. M. Effects of Coke Deposits on the Catalytic Performance of Large Zeolite H-ZSM-5 Crystals during Alcohol-to-Hydrocarbon Reactions as Investigated by a Combination of Optical Spectroscopy and Microscopy. *Chem. - Eur. J.* **2015**, *21* (48), 17324−17335.
(84) Castaño, P.; Ruiz-Martínez, J.; Epelde, E.; Gayubo, A. G.; Weckhuysen, B. M. Spatial Distribution of Zeolite ZSM-5 within Catalyst Bodies Affects Selectivity and Stability of Methanol-to-Hydrocarbons Conversion. *ChemCatChem* **2013**, *5* (10), 2827−2831.
(85) VanSpeybroeck, V.; Hemelsoet, K.; DeWispelaere, K.; Qian, Q.; VanderMynsbrugge, J.; DeSterck, B.; Weckhuysen, B. M.; Waroquier, M. Mechanistic Studies on Chabazite-Type Methanol-to-Olefin Catalysts: Insights from Time-Resolved UV/Vis Micro-spectroscopy Combined with Theoretical Simulations. *ChemCatChem* **2013**, *5* (1), 173−184.
(86) Mores, D.; Kornatowski, J.; Olsbye, U.; Weckhuysen, B. M. Coke Formation during the Methanol-to-Olefin Conversion: In Situ Microspectroscopy on Individual H-ZSM-5 Crystals with Different Brønsted Acidity. *Chem. - Eur. J.* **2011**, *17* (10), 2874−2884.
(87) Hemelsoet, K.; Qian, Q.; De Meyer, T.; De Wispelaere, K.; De Sterck, B.; Weckhuysen, B. M.; Waroquier, M.; Van Speybroeck, V. Identification of Intermediates in Zeolite-Catalyzed Reactions by in Situ UV/Vis Microspectroscopy and a Complementary Set of Molecular Simulations. *Chem. - Eur. J.* **2013**, *19* (49), 16595−16606.

https://dx.doi.org/10.1021/acssuschemeng.0c07153
ACS Sustainable Chem. Eng. XXXX, XXX, XXX−XXX